Journal of Petroleum Exploration and Production Technology
https://doi.org/10.1007/s13202-024-01794-8

ORIGINAL PAPER-PRODUCTION ENGINEERING

New correlations to estimate the rough fracture permeability using computational fluid dynamics simulation

Farshid Valizadeh[1] · Mojtaba Ghaedi[1] · Sara Hemmati[2] · Mehrzad Feilizadeh[2] · Hamid Garmsiri[1]

Received: 28 June 2023 / Accepted: 16 March 2024

Abstract

In fractured reservoirs, the fracture network provides the main path for fluid flow. Appropriate estimation of the fracture permeability influences the precise prediction of the reservoir's future performance. Commonly, for a known geometry of natural or induced fracture, the permeability is estimated by applying local cubic law. One major drawback of this approach is that the fracture surface roughness, which has a significant effect on fracture permeability, is not considered. Moreover, the knowledge about the impact of fracture surface roughness on fracture permeability is not currently sufficient. In this research, the fluid flow in fractures with rough-walled surfaces was studied using computational fluid dynamics. For this purpose, the fluid flow through fractures was simulated by applying appropriate roughness for fracture walls. Furthermore, two correlations, based on response surface methodology and power-law models, were proposed to predict fracture permeability as a function of four independent variables (surface roughness, fracture aperture, angle, and porosity). The results of the two presented correlations were validated, and the statistical analysis indicates that both models are appropriate to predict fracture permeability. The findings of this study will be of great assistance with understanding and characterization of the fluid flow in rough fractures and can be used in future works.

Keywords Fracture permeability · Surface roughness · Computational fluid dynamics · Local cubic law · Response surface methodology

List of symbols

Latin letters

a	Amplitude (m)
a_1	Power-law parameters
b	Fracture aperture (µm)
c_i	Power-law parameter i
D_{f}	Fracture dimension
E_t	Relative error
f_i	Frequency
g	Gravitational acceleration (m/s^2)
h	Matrix height (m)
H	Hurst exponent
k	Fracture permeability (D)
L	Length of fracture (m)
L_{sinewave}	Actual length of the fracture (m)
P	Pressure (Pa)
R^2	Coefficient of determination
r_f	Geometric sequence ratio
u	Fluid velocity (m/s)
V_{fracture}	Fracture volume (m^3)
V_{matrix}	Matrix volume (m^3)
WL	Wavelength (m)
$\mathrm{WL}_{\max}$	Maximum wavelength (m)
x	Abscissa (m)
x_0	Phase of the sine wave (m)
$x_{i.0}$	Random phase of the sinewave (m)
y	Ordinate (m)

Greek letters

β_0	Interception coefficient
β_i	Coefficient of independent variable i
β_{ii}	Quadratic coefficients
β_{ij}	Interaction terms
θ	Angle between the fracture and flow direction (°)
φ	Porosity
ρ	Fluid density (kg/m^3)

✉ Mojtaba Ghaedi
m.ghaedi@shirazu.ac.ir

[1] Department of Petroleum Engineering, School of Chemical and Petroleum Engineering, Shiraz University, Shiraz, Iran

[2] Department of Chemical Engineering, School of Chemical and Petroleum Engineering, Shiraz University, Shiraz, Iran

μ	Fluid viscosity (Pa.s)
Φ	Fluid potential (pa)

Abbreviations

AAD	Absolute average deviation
ANOVA	Analysis of variance
CCD	Central composite design
CFD	Computational fluid dynamics
FMI	Formation micro imager
FZI	Flow zone indicator
LCL	Local cubic law
LBM	Lattice Boltzmann methods
MAE	Mean absolute error
NSE	Navier-Stokes equation
Re	Reynold's number
RSM	Response surface methodology
RMSE	Root mean square error
SRF	Surface roughness factor

Introduction

A high percentage of world reservoirs are naturally fractured reservoirs and these reservoirs contain a significant amount of oil and gas in the world (Ghaedi et al. 2015). Also, it is common to use artificial hydraulic fracturing in tight reservoirs to improve oil recovery (Xu et al. 2021). Hydraulic fracturing is one of the main methods to increase the recovery factor of shaly reservoirs by artificial fractures, which increase the permeability of the shale zone (Guo et al. 2020; Zhang and Hascakir 2021). The presence of natural or induced fractures significantly affects the mechanical properties of rocks, such as permeability (Li et al. 2021). Moreover, in tight rocks such as clay, fluid flow through pores is insignificant compared with fractures. Also, in the reservoirs, fractures act like microchannels and are the flow path of the fluid (Abbasi et al. 2016). Thus, proper characterization of fluid flow in these channels is a priority in the oil industry, geology, and hydrogeology and can be beneficial in artificial hydraulic fracturing and naturally fractured reservoir production (Lei et al. 2022).

Due to the great impact of fracture permeability on fluid flow in porous media, the proper determination of this parameter is of great importance (Hou et al. 2021) to reduce the geological uncertainty in the model (Yousefzadeh and Ahmadi 2023; Yousefzadeh et al. 2023). Patel et al. (2018) took benefit from the diffusion equation to estimate the hydraulic fracture permeability based on recorded pressure data just after the breakdown during hydraulic fracturing. Well testing and well logging are two of the conventional methods used for estimating the fracture permeability (Laongsakul and Dürrast 2011; Mazaheri et al. 2015; Shalaby and Islam 2017). Bagheri and Falahat (2022) used conventional well logs and flow zone indicator (FZI) to estimate facture permeability. In this method, first, the properties of open fractures such as their aperture, density, porosity, and permeability are approximated by Formation Micro Imager (FMI) logs. Then, conventional logs (density, micro-resistivity, sonic, and caliper logs) are used to estimate the fracture index log, which is used to estimate the fracture permeability from the FZI equation. Freites et al. 2019) used well testing results to derive the permeability of natural fractures with disconnected and heterogeneous fractures. However, well testing and well logging are expensive and time-consuming. Thereby, other analytical and numerical methods have been in the focus of researchers.

Local cubic law (LCL) has been used frequently to relate the fracture permeability to fracture opening, thickness, and angle. However, many studies have shown that the LCL cannot correctly estimate fracture permeability (Tsang and Witherspoon 1981; Madadi and Sahimi 2003; Deng et al. 2018). This is because many complexities of fracture geometry are not considered in LCL. The main problem with LCL is that it fails to take surface roughness into account. Several studies have been performed to investigate the effect of fracture roughness. Gutfraind and Hansen (1995) studied the permeability of rough fractures using Lattice Gas Automata. They modeled the fractures with a channel that was bounded with a rough and the other side with a smooth plane parallel to the flow direction. Due to the symmetry effect, they showed that the internal surface should be a mean smooth plane. (Zhang et al. 1996) simulated the fluid flow through 3D fractures and found that the effective permeability (k) and mean aperture (b) have a relationship of $k \sim b^{\beta}$ where β is a power varying from 2 to 6.

Along with numerical simulations, (Skjetne et al. 1999) computed fluid flow through fractures using the finite difference method for a wide range of Reynold's Numbers (Re). They concluded that the narrowest aperture perpendicular to the flow would controls the effective permeability in low Re values. Based on LCL, Talon et al. (2010) widened the bottleneck effect. They noticed that the fracture permeability must be described for different flow regimes by considering the ratio of roughness to mean aperture. The size and the shape of the roughness irregularities will affect the whole flow characteristics with respect to the fracture aperture (Tsang et al. 1988; Murata and Saito 2003). Moreover, Wang et al. (2016) studied the impact of the multi-scale surface roughness on fluid flow through rough fractures by using Lattice Boltzmann Methods (LBM). Their results showed that the roughness dominates the flow direction and pressure distribution.

Recently, Deng et al. (2018) have investigated the effect of fracture roughness on reaction rate and concluded that by increasing the surface roughness, the hydraulic tortuosity increases, and fracture permeability reduces. According to fracture models analyzed via computational fluid dynamics (CFD) by COMSOL simulations, Sarkar et al. (2004) have proposed some modifications for LCL for parallel and series fracture networks separately. For inclined fractures concerning the flow direction, they observed that the fracture permeability would be multiplied by a factor of cosine and not by a factor of cosine^2. Wang et al. (2022) coupled the PFC2D with COMSOL Multiphysics to investigate hydraulic fracturing on coal seam permeability. Their results showed that by increasing the fracturing time, the difference between the vertical and horizontal fractures increases as well. COMSOL Multiphysics is solver, finite element analysis, and simulation software package that can be used to solve different physics and engineering problems, especially coupled phenomena and multiphysics.

Guo et al. (2020) investigated experimentally the fluid flow through artificially rough-walled fractures and observed that fracture roughness creates eddies in fluid flow. The eddies result in shrinking the effective channel and making the fluid flow nonlinear. In addition, Liu et al. (2016) investigated the effect of fracture roughness on fluid flow experimentally and numerically. They concluded that the origin of the nonlinearity of fluid flow is the inertia effect due to the surface roughness. Briggs (2014) studied the impact of the roughness on fluid flow by simulating two-dimensional rough fracture fluid flow using LBM. The results of LBM showed a significant deviation from the results of conventional cubic law. Additionally, using CFD simulations, a new model, which suggests a polynomial expression like Forchheimer's law, was proposed for nonlinear fluid flow through rough fractures (Javadi et al. 2010). The non-Darcy flow thorough single rough fracture simulation results indicates that the cubic law fails to predict the flow compared with experimental and LBM results (Ju et al. 2017).

Based on the performed simulation studies on fracture flow, it was observed that LCL overestimates the flow rate in rough fractures and also the surface roughness geometry should be considered in the studies (Wang et al. 2015; Toghraie et al. 2019). Wang et al. (2015) proposed a modified LCL, which includes roughness, to predict the fluid flow through real fractures. The experimental results confirmed the superiority of the modified LCL to general LCL.

As mentioned previously, LCL could not be applied to estimate the fracture permeability since the fracture surface roughness is not considered. Therefore, to investigate the effect of roughness on fracture permeability, comprehensive studies and statistical analyses are required. For this purpose, Response surface methodology (RSM) can be used. Because RSM is a useful modeling method that is applied as a statistical approach to design experiments and to develop a polynomial-based model (Feilizadeh et al. 2015a). Moreover, insignificant parameters of this model can be easily found (Mohammadi et al. 2014).

Although the previous studies give a valuable vision into the fluid flow through rough fractures, this situation has not been comprehensively studied. Also, fracture permeability in the presence of rough fracture has not been studied accurately. Therefore, this study has explored fluid flow through rough apertures in detail using COMSOL Multiphysics, and all the parameters such as gravity, porosity, and fracture opening that can affect fracture permeability were examined. Due to the fact that the studied model is 2D and parameters like tortuosity need to be defined in a 3D model, these kinds of parameters' effects were not examined. Finally, new correlations to precisely calculate the permeability of rough fractures have been proposed after verifying the main parameters. Moreover, the performance of the proposed correlations was tested by some new models and was compared with the estimated permeabilities from LCL.

Theory

The following assumptions were considered in constructing the model and simulations in this study:

- The flow was laminar and single phase.
- The model was two-dimensional, and the effect of tortuosity on fluid flow was not considered.
- The flow was considered dual porosity and single permeability (i.e., it was assumed that fluid flow only occurred in fractures).
- Block to block interactions were ignored.

Governing equations

The governing equations for laminar flow through microchannel are Navier–Stokes Equation (NSE) and mass conservation, which are (Versteeg 1995):

$$\rho(u \cdot \nabla)u = -\nabla P + \mu \nabla^2 u \tag{1}$$

$$\nabla \cdot u = 0 \tag{2}$$

where ρ is the fluid density, u is fluid velocity, P is pressure, and μ is fluid viscosity. It is common to assume two separated smooth parallel plates with a constant aperture when modeling fluid flow through fractures (Snow 1969). Under this assumption and using lubrication theory, the LCL can be derived from NSE, which takes the form of (Zimmerman et al. 1991; Wang et al. 2018):

$$\nabla \cdot \left[\frac{\rho g b^3}{12\mu} \nabla \Phi\right] = 0 \tag{3}$$

where g is the gravitational acceleration, b is fracture aperture, and Φ is fluid potential.

Using the Darcy equation and LCL; fracture permeability in a matrix–fracture system would be resulted in (Golf-Racht 1982):

$$k = \frac{b^3 \cos^2 \theta}{12h} \tag{4}$$

where k is fracture permeability, θ is the angle of fracture with the flow direction, and h is the matrix height.

On the other hand, Sarkar et al. (2004) simulated fluid flow through fractures using COMSOL Multiphysics and observed that for smooth fractures, the permeability formula would be:

$$k = \frac{b^3 \cos \theta}{12h} \tag{5}$$

Methodology

Rough profiles generation

Previous studies have pointed out some techniques to characterize wall roughness (Barton and Choubey 1977; Crandall et al. 2010). Three main methods are the joint roughness coefficient, the fractal dimension (D_f), and the surface roughness factor (SRF). The Hurst exponent (H) is the fractal dimension which is in relation to the fractal dimension as (Deng et al. 2018):

$$D_f = 2 - H \tag{6}$$

where H can be calculated via the variable-bandwidth technique. In this study, the SRF method has been used to characterize aperture surface roughness. In the following, this method is discussed in detail (Deng et al. 2018).

2D matrix–fracture systems for single fractures can be considered to simulate fluid flow through rough fractures. 2D rough profiles are obtained by overlaying a series of sine waves. Each fracture is formed from a rough profile and its mirror symmetry. By considering the sine waves, three rough profiles would be produced, which are single sine wave, self-similar, and self-affine (Fig. 1) (Li et al. 2008; Deng et al. 2018).

A single sine wave creates an ideal rough profile and is generated via the below equation (Deng et al. 2018):

$$y = a \times \sin\left(\frac{2\pi}{WL}\left(x - x_0\right)\right) \tag{7}$$

where x is abscissa, y and a represent the ordinate and amplitude, respectively. WL indicates the wavelength, and x_0 is the phase of the sine wave. This simple profile is applied

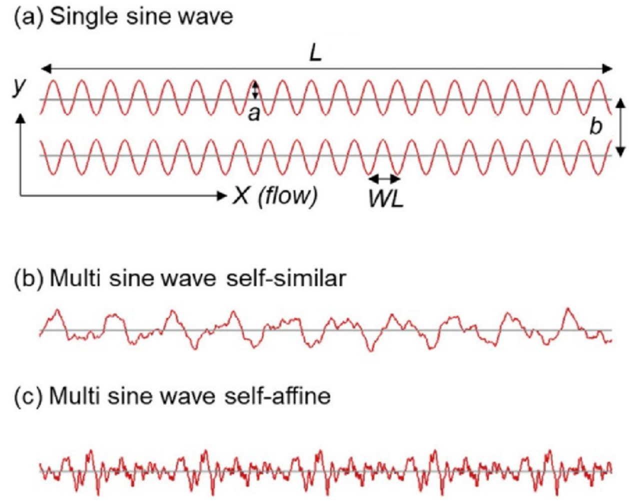

Fig. 1 A scheme of three types of rough profiles **a** Single sine wave rough profile with a WL = 50 μm and a = 30μm **b** self-similar rough profile (lower half of the aperture) **c** self-affine rough profile (lower half of the aperture) (Deng et al. 2018)

extensively and observed that is extremely applicable to investigate flow through rough fractures (Bouquain et al. 2012; Sund et al. 2015).

The second and third profiles are known as fractal profiles generated by overlaying a series of sinewaves. It is common to use fractal profiles to describe rough fractures and faults in oil fields and laboratories (Power and Tullis 1991; Meakin 1993; Glover et al. 1998; Renard et al. 2013). These profiles can be generated via the below equation:

$$y = \sum_i a_i \times \sin\left(f_i\left(x - x_{i.0}\right)\right) \tag{8}$$

where $f_i = \frac{2\pi}{\mathrm{WL}_i}$ is the frequency and $x_{i.0}$ is the random phase of the sinewave.

In Eq. (3), if f_i follows a geometric sequence, the generated profile will be self-similar, and if f_i follows an arithmetic sequence, the generated profile will be self-affine (Deng et al. 2018). In this study, self-similar profiles were used to create rough apertures that the frequencies follow a geometric sequence as below (Deng et al. 2018):

$$f_i = \frac{2\pi}{\mathrm{WL}_{\max}} r_f^{i-1} \tag{9}$$

where $\mathrm{WL}_{\max}$ is the maximum wavelength and r_f is the geometric sequence ratio. It is necessary to notice that all the parameters that control the rough profiles are generated randomly. To ensure that the rough aperture is open, only profiles are considered that $y_{\max} < \frac{b}{2}$ (Renard et al. 2004).

As mentioned previously, to characterize fractures roughness, the SRF method was used, which is defined as the ratio of the actual length of the fracture ($L_{sinewave}$) to the geometric length of fracture (L) (Deng et al. 2018):

$$SRF = \frac{L_{sinewave}}{L} \tag{10}$$

Model set-up

Matrix with a length of 2000 microns was considered to generate models of the matrix–fracture system. Since porosity, opening, and fracture angles were considered as the main parameters, the matrix height was calculated from the following equation (Golf-Racht 1982):

$$h = \frac{100 \times b}{\varphi \times \cos\theta} \tag{11}$$

where φ indicate fracture opening and the porosity in percent. Because in the studied model the matrix zone is impermeable and only the fracture contributes to the flow, the porosity in this study refers to the fracture porosity. Hereby, the definition of fracture porosity would be as below (Golf-Racht 1982):

$$\varphi = \frac{V_{fracture}}{V_{matrix} + V_{fracture}} \times 100 \tag{12}$$

where $V_{fracture}$ and V_{matrix} show fracture and matrix volumes, respectively. The matrix–fracture system was considered an element of a fracture network (Golf-Racht 1982), so the entrance domain to the fracture itself is also a vertical fracture. Since the matrix zone was assumed as an impermeable zone, the matrix zone was deleted in the final geometry. For example, the geometry of a matrix–fracture geometry with $SRF = 2.0$, $b = 150$ µm, $\varphi = 11\%$, and $\theta = 30$ ° is shown in Fig. 2.

After generating the geometry, the fluid type or properties should be defined. Except for gas flow near the wellbore, the fluid flow for most of the cases in the reservoirs is laminar (Tarek 2010). Therefore, in this study, water, which is an incompressible liquid and the laminar flow, was considered to simulate the fluid flow through the fracture. A steady-state regime was used, as the conditions of the fluid are constant in this situation. For the boundary conditions, the inlet boundary was defined as a normal inflow velocity with a velocity of 1 ft/d, and the outlet boundary was defined as a constant pressure boundary with a pressure of 4000 psi. The other boundaries (which illustrate fracture-matrix fluid exchange) were defined as *the no-slip* boundary because of the impermeable matrix assumption.

Finally, after generating the model in the COMSOL Multiphysics, the fluid flow through fracture was simulated. As instance, Figs. 3 and 4 demonstrate the pressure and velocity distributions for different fracture characteristics.

After the simulation, the averaged fluid velocity and the average fluid pressure at the inlet and outlet boundaries were calculated. Then, using the Darcy equation and the calculated

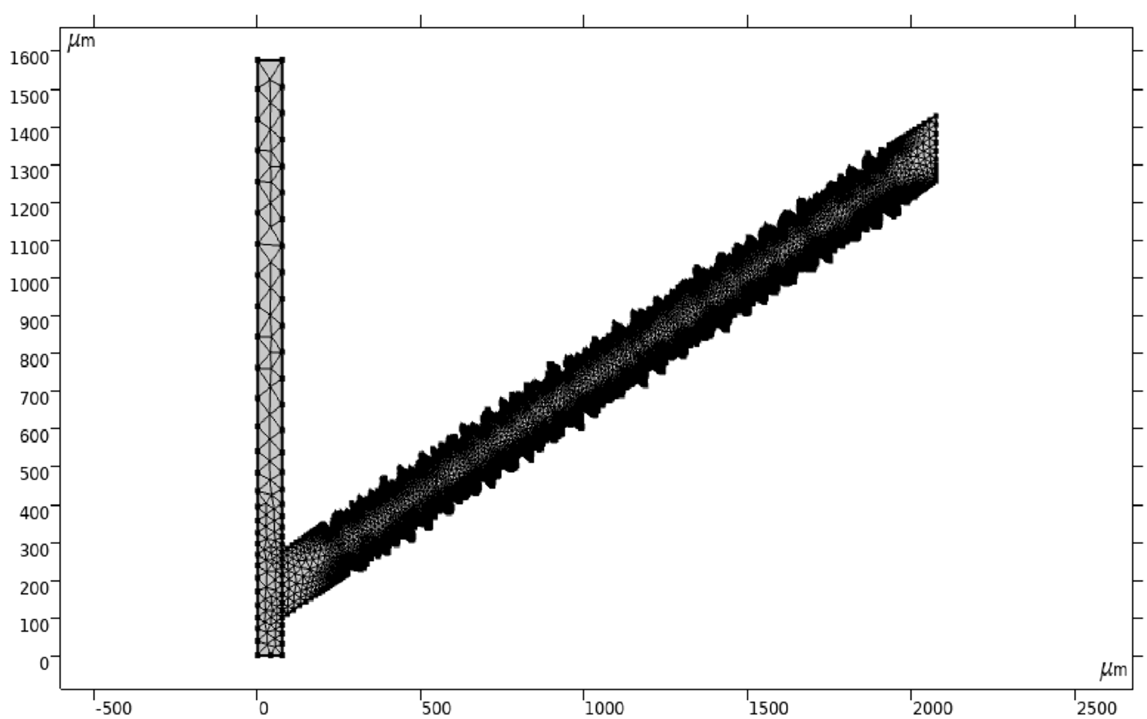

Fig. 2 The meshed geometry for a fracture with SRF = 2.0, $b = 150$ µm, $\varphi = 11\%$, and $\theta = 30°$

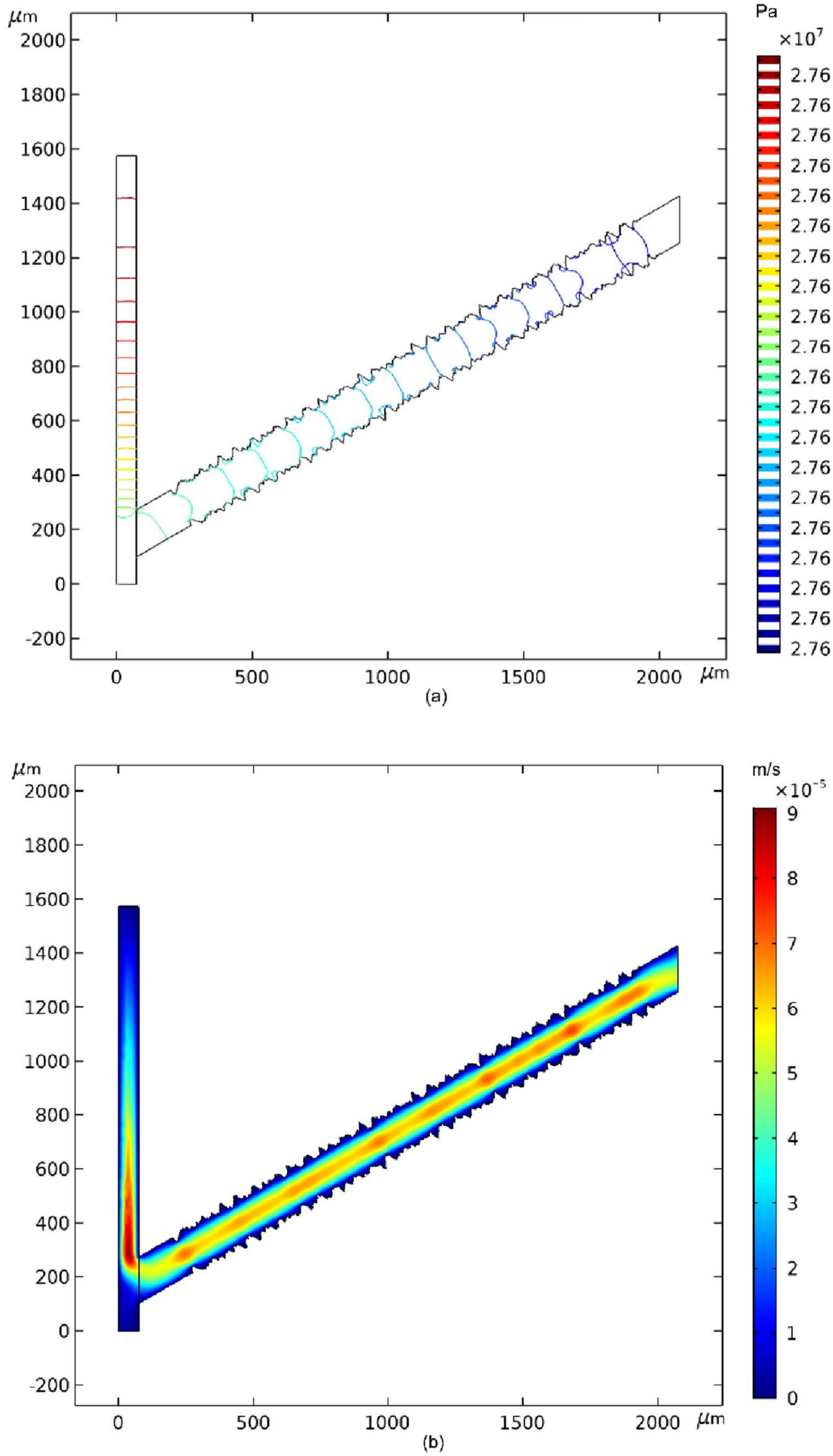

Fig. 3 **a** Contour plot of pressure distribution **b** heat map of velocity distribution for a fracture with SRF = 2.0, b = 150 μm, φ = 11%, and θ = 30°

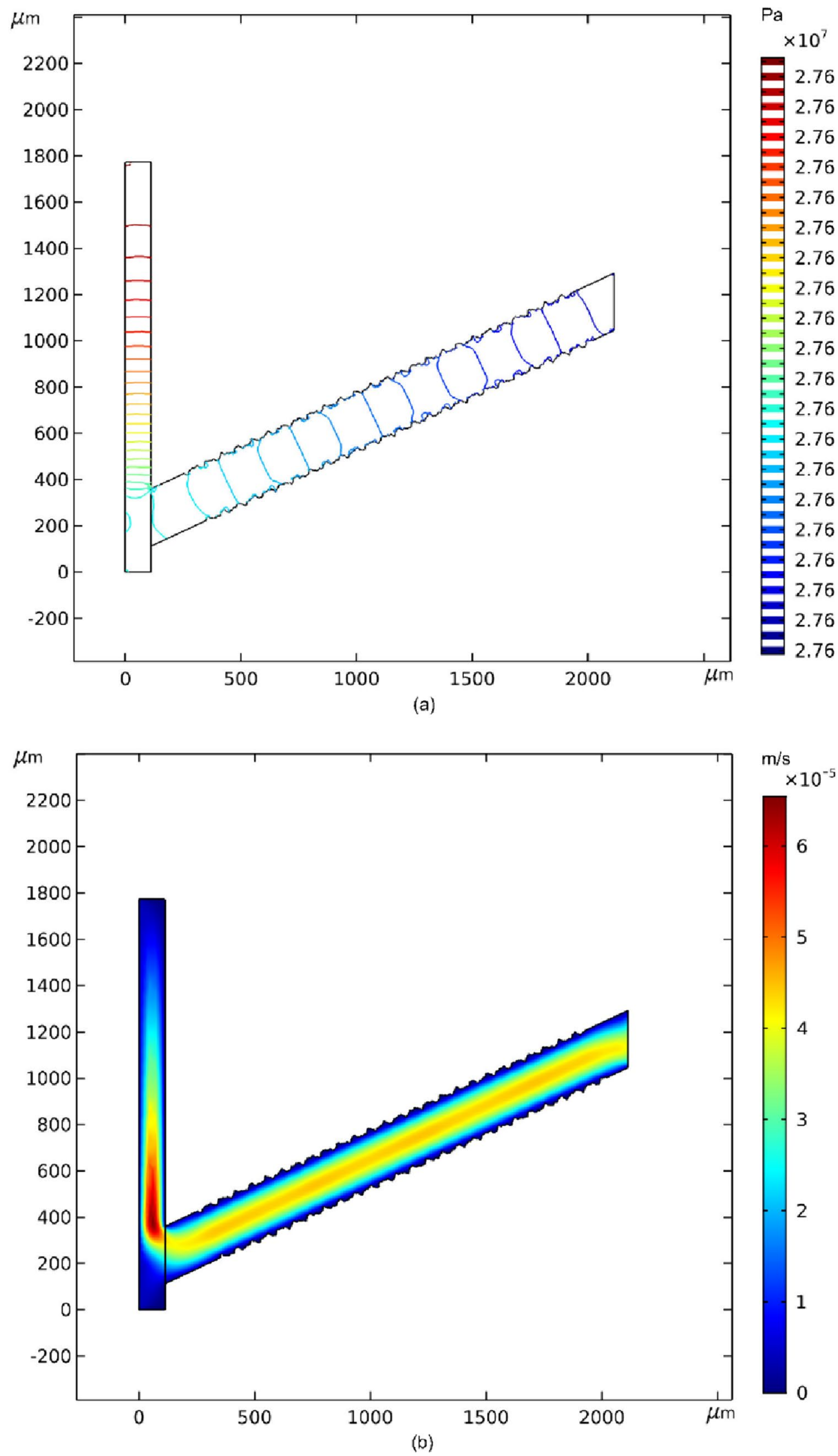

Fig. 4 **a** Contour plot of pressure distribution **b** heat map of velocity distribution for a fracture with SRF = 1.5, b = 225 μm, φ = 14%, and θ = 25°

average parameters from the simulation results, the fracture permeability was calculated for every model.

Design and analysis of experiments

The impact of rock and fluid properties on fracture permeability was studied. Among the examined parameters, the only parameters that affect the fracture permeability were fracture opening, porosity, SRF, and fracture angle with the flow direction. In this study, the central composite design (CCD) was used to perform the design of tests. This method designs a limited number of tests. To increase the final correlation accuracy, a large number of tests should be designed (Bararpour et al. 2018). Four series of experiments were designed to generate 120 tests (simulation models).

In the RSM model, the fracture permeability could be fitted to a polynomial-based model as a function of the four independent variables (Eq. (12)).

$$\sqrt{k} = \beta_0 + \beta_1 \times \mathrm{SRF} + \beta_2 \times b + \beta_3 \times \theta + \beta_4 \times \varphi + \beta_{12} \times \mathrm{SRF} \times b + \beta_{13} \times \mathrm{SRF} \times \theta + \beta_{14} \times \mathrm{SRF} \times \varphi + \beta_{23} \times b \times \theta + \beta_{24} \times b \times \varphi + \beta_{34} \times \theta \times \varphi + \beta_{11} \times \mathrm{SRF}F^2 + \beta_{22} \times b^2 + \beta_{33} \times \theta^2 + \beta_{44} \times \varphi^2 \quad (13)$$

where k is the fracture permeability as the response in Darcy, SRF is dimensionless, b and θ are in microns and degree, respectively, and φ is in percent. Moreover, β_0 demonstrates the interception coefficient, β_1, β_2, $\beta_{3,}$ and β_4 are the coefficient of independent variables, β_{12}, β_{13}, β_{14}, β_{23}, β_{24}, and β_{34} are the interaction terms and β_{11}, β_{22}, β_{33} and β_{44} are quadratic coefficients. Furthermore, the analysis of variance (ANOVA) was carried out by the Design-Expert® Software (Trial Version 11.1.1.0 Stat-Ease, Inc. Minneapolis, USA). The ANOVA has provided a useful tool to investigate the effect of variables on the response (Feilizadeh et al. 2017).

Results and discussion

Smooth fracture permeability

As mentioned in the introduction section, the LCL is derived from the Navier–Stokes Equations. One way to verify the validity of the constructed simulation model is to compare the results of the COMSOL simulation with the results of the LCL for a smooth fracture with no angle. If the results match, the constructed model is valid. Table 1 reports the results of permeability calculation for a smooth fracture with different apertures and porosities. As shown, there is an excellent agreement between the results of the CFD simulation (COMSOL) and the LCL. Thereby, the constructed simulation model is valid.

Another comparison is made for a smooth fracture with constant opening, but with different angles. The results are shown in Table 2. The CFD results are compared with LCL and Eq. (5) (Sarkar et al. 2004), and it is found that the permeabilities from CFD results are in agreement with Eq. (5). These results confirm the validity of the constructed model for fracture permeability analysis.

Table 1 Calculated permeabilities by the LCL and CFD (COMSOL) for smooth fractures with no angle

Fracture opening (μm)	Porosity (%)	CFD perm. (D)	LCL perm. (D)	Difference between CFD and LCL perm. (%)
100	20	168.72	168.87	0.09
150	5	94.19	94.99	0.85
200	15	507.01	506.62	0.08
250	10	528.31	527.73	0.11

Table 2 Calculated permeability of smooth fractures with LCL and Eq. (5)

SRF	L (mμ)	Fracture opening (mμ)	Angle (deg)	Porosity (%)	CFD perm. (D)	LCL perm. (D)	Equation (5) perm. (D)
1	2000	150	20	10	164.2	157.6	167.8
1	2000	150	25	10	153.6	141.4	156.1
1	2000	150	30	10	139.6	123.4	142.5
1	2000	150	35	10	126.1	104.4	127.5
1	2000	150	40	10	109.3	85.40	111.5

RSM model

All the 120 designed tests were simulated, and the permeabilities of the models were calculated. The calculated permeabilities were analyzed via Design-Expert® Software (Trial Version 11.1.1.0 Stat-Ease, Inc. Minneapolis, USA), and the following RSM model was obtained.

$$\sqrt{k} = -2.16 + 0.149 \times \mathrm{SRF} + 0.0613 \times b - 0.00232 \times \theta + 0.486 \times \varphi - 0.00135 \times \mathrm{SRF} \times b + 0.0518 \times \mathrm{SRF} \times \theta - 0.137 \times \mathrm{SRF} \times \varphi - 0.000443 \times b \times \theta + 0.00382 \times b \times \varphi - 0.000939 \times \theta \times \varphi - 0.663 \times \mathrm{SRF}^2 - 6.06 \times 10^{-6} \times b^2 - 0.00252 \times \theta^2 - 0.0128 \times \varphi^2 \tag{14}$$

Results of ANOVA for the obtained model (Eq. 13) are presented in Table 3. It can be seen that a few terms have a high p-value (higher than 0.05), and therefore, they have an insignificant effect on the response (permeability) and can be omitted. It is noticeable that the square of the fracture opening (b) term can be neglected due to the high p-value. This is consistent with LCL where the permeability has a relationship with the square of the fracture opening. By omitting the parameters that have insignificant effects, the modified correlation (as the RSM model) would be as follows.

$$\sqrt{k} = -2.23 + 0.199 \times \mathrm{SRF} + 0.0582 \times b + 0.0175 \times \theta + 0.504 \times \varphi + 0.0416 \times \mathrm{SRF} \times \theta - 0.157 \times \mathrm{SRF} \times \varphi - 0.000514 \times b \times \theta + 0.00372 \times b \times \varphi - 0.641 \times \mathrm{SRF}^2 - 0.00231 \times \theta^2 - 0.0118 \times \varphi^2 \tag{15}$$

The ANOVA of the modified model is presented in Table 4. The p-values of the parameters indicate that all of them have a significant effect. Moreover, the F-value of the new RSM model is 21,234 which is much greater than the previous one and represents the adequacy of the model (Feilizadeh et al. 2015b). In addition, the statistical analysis of the RSM model is shown in Table 5. The values of R^2 and R^2-adjusted are higher than 0.99 which signifies that the RSM model is appropriate to predict fracture permeability. Furthermore, the values of root mean square error (RMSE), mean absolute error (MAE), and absolute average deviation (AAD) also show the high accuracy of the RSM model. The obtained and predicted values of the fracture permeability are plotted in Fig. 5. As seen in this figure, the RSM model has a superior ability to predict the system.

Table 3 ANOVA of the RSM model before omitting insignificant parameters

Source	Sum of squares	Mean square	F-value	p-value
Model	24,819	1773	16,842	< 0.0001
A-SRF	126.2	126.2	1199	< 0.0001
B-opening (b)	3269	3269	31,055	< 0.0001
C-angle (θ)	38.39	38.39	364.7	< 0.0001
D-porosity (φ)	417.4	417.4	3965	< 0.0001
AB	0.17	0.17	1.61	0.2074
AC	2.04	2.04	19.34	< 0.0001
AD	3.99	3.99	37.89	< 0.0001
BC	5.92	5.92	56.28	< 0.0001
BD	113.8	113.8	1080	< 0.0001
CD	0.05	0.05	0.49	0.4864
A^2	1.67	1.67	15.89	0.0001
B^2	0.21	0.21	1.95	0.1650
C^2	3.15	3.15	29.96	< 0.0001
D^2	8.97	8.97	85.22	< 0.0001
Residual	11.05	0.11		
Lack of fit	11.05	0.13		
Pure error	0.00	0.00		
Cor total	24,830			

Table 4 ANOVA of the RSM model after omitting insignificant parameters

Source	Sum of squares	Mean square	F-value	p-value
Model	24,819	2256	21,235	< 0.0001
A-SRF	141.53	141.5	1332	< 0.0001
B-opening (b)	4436	4436	41,750	< 0.0001
C-angle (θ)	68.91	68.91	648.6	< 0.0001
D-porosity (φ)	834.6	834.6	7855	< 0.0001
AC	2.02	2.02	19.00	< 0.0001
AD	9.37	9.37	88.20	< 0.0001
BC	16.43	16.43	154.7	< 0.0001
BD	224.15	224.2	2110	< 0.0001
A^2	1.58	1.58	14.86	0.0002
C^2	3.55	3.55	33.40	< 0.0001
D^2	14.22	14.22	133.8	< 0.0001
Residual	11.48	0.11		
Lack of fit	11.48	0.13		
Pure error	0.00	0.00		
Cor total	24,830			

Table 5 The statistical analysis of the RSM model

Statistical parameters	Value
R^2	0.9992
R^2_{adj}	0.9992
RMSE	20.06
MAE	11.24
AAD	5.141

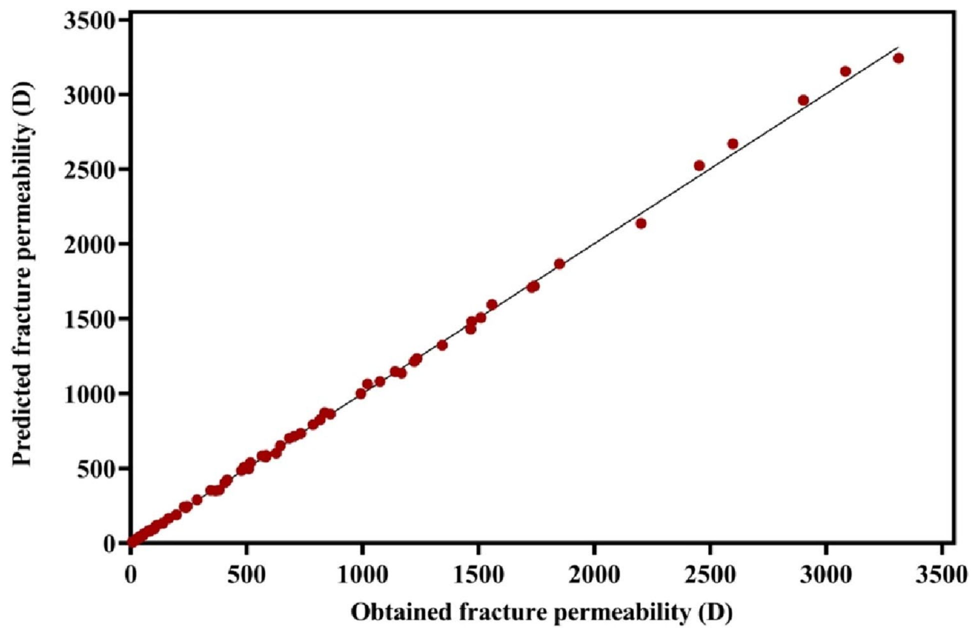

Fig. 5 The plot predicted fracture permeability versus obtained fracture permeability

Table 6 Constant values

Power-law parameters	Value
a_1	0.000225
c_1	0.000100
c_2	2.19
c_3	2.09
c_4	1.01

Power-law model

As described before, fracture permeability can be described as a function of SRF, opening (b), angle (θ), and porosity (φ). To develop a relationship between permeability and the mentioned parameters, the power-law equation (which is a modified form of LCL) was utilized as follows.

$$k = a_1 \times (\mathrm{SRF}^{c_1} \times b^{c_2} \times (\cos\theta)^{c_3} \times \varphi^{c_4}) \tag{16}$$

where a_1, c_1, c_2, c_3, and c_4 are constants of the equation. The values of constants were optimized by using the genetic algorithm and are presented in Table 6.

By finding the values of constants from the genetic algorithm, the power-law equation was obtained (Eq. 12).

$$k = 0.000225 \times \left(\mathrm{SRF}^{0.000100} \times b^{2.19} \times (\cos\theta)^{2.09} \times \varphi^{1.01}\right) \tag{17}$$

Table 7 The statistics of the power-law equation

Statistical parameters	Value
R^2	0.9886
R^2_{adj}	0.9882
RMSE	77.18
MAE	40.75
AAD	14.51

The statistical analysis of the obtained power-law equation is shown in Table 7. The value of R^2 and R^2-adjusted was found to be 0.9886 and 0.9882, respectively. These values indicate that the power-law equation could be used to predict fracture permeability.

Correlations validity

It is essential to check the validity of the new correlations. One way of validation is to compare the correlation's predictions with the true value of new experiments or numerical simulations. In this study, as no good experimental data with specified fracture were not found in the literature, similar to Rezaei Niya and Selvadurai (2019), the calculated permeability directly from CFD COMSOL Multiphysics has been considered as the true value. For this purpose, 12 new models were generated randomly to simulate and calculate the true values.

The results of the three models are summarized in Table 7. The relative errors of predictions of LCL, the RSM model, and the power-law model were also calculated and presented in Table 8. The results show that the RSM model and power-law model have higher accuracy

Table 8 Properties of the test models and the results of CFD, LCL, RSM model, and the power-law model

Model	SRF	Opening (mμ)	Angle (deg)	Porosity (%)	CFD perm. (D)	LCL perm. (D)	RSM perm. (D)	Power-law perm. (D)	$\%E_t$ (LCL)	$\%E_t$ (RSM)	$\%E_t$ (Power-law)
1	1.46	220	4	23	787.2	935.4	796.3	718.5	18.82	2.280	8.730
2	1.25	75	5	11	40.57	51.85	42.28	32.22	27.81	4.220	20.59
3	2.15	135	27	5	30.01	61.09	29.83	41.70	103.5	0.6000	38.93
4	2.25	115	27	7	24.05	62.06	23.52	41.22	158.0	2.210	71.37
5	1.65	75	0	14	32.07	66.49	32.94	41.48	107.3	2.700	29.17
6	2.35	135	17	7	41.94	98.51	42.81	67.91	134.9	2.070	61.91
7	1.46	190	0	18	448.9	548.7	466.2	409.0	22.23	3.870	8.890
8	1.46	260	8	28	1356	1567	1351	1244	15.57	0.4000	8.260
9	2.15	190	4	28	501.8	849.3	462.1	635.6	69.25	7.930	26.66
10	2.35	145	27	3	19.98	42.28	19.90	29.12	111.7	0.3700	45.76
11	1.25	95	11	14	84.90	102.8	89.00	66.88	21.10	4.830	21.23
12	1.65	95	5	8	34.71	60.50	36.46	39.20	74.31	5.050	12.95

Table 9 The statistics of the models

Statistical parameters	LCL	RSM	Power-law
R^2	0.9194	0.9992	0.9849
R^2_{adj}	0.9166	0.9992	0.9844
RMSE	130.9	12.96	56.62
MAE	86.99	6.796	38.22
AAD	37.02	2.923	22.97

than the LCL to estimate fracture permeability. In addition, the statistical analysis of the models is presented in Table 9, and as can be seen, R^2 of the RSM model and power-law model are closer to 1 compared to the LCL. The value of RMSE calculated for the RSM model is less than others. Therefore, the RSM model has good predictive ability than the power-law equation, and thus, RSM model has the most accuracy.

However, to have better insights into the impacts of roughness, experimental investigations are highly recommended.

Effect of parameters on the permeability

The impact of the main parameters on the permeability was obtained using the RSM model (the most accurate model, Eq. (14)). Figure 6 indicates that in the constant value of b and φ, the permeability decreases by increasing SRF and θ. It is evident that by increasing the SRF, the friction of the flow and, as a result, the pressure drop would increase. The real length of the fracture, which is the path of the flow, can be calculated from the following equation:

$$L_{\text{fracture}} = \frac{L}{\cos\theta} \tag{18}$$

It is evident from Eq. (18) that by increasing θ, the fracture length increases and the fluid would result in more pressure drop, which is the driving force in the fluid flow. Therefore, increasing SRF and θ would decrease the permeability.

Figure 7 shows the effect of SRF and φ in the constant value of b and θ. The SRF effect was discussed before. As can be seen from this figure, φ and permeability are directly related to each other. For the φ impact, the figure shows that increasing φ causes the enhancement of the permeability. By increasing φ, the inlet area would increase as also the volume of the inlet fluid. A higher amount of the fluid would support the flow, and as a result, the pressure drop through the fracture would significantly decrease, and the permeability would increase (Lemonnier and Bourbiaux 2010).

The effect of b and θ, in the constant value of SRF and φ, is demonstrated in Fig. 8. As discussed previously, permeability and θ have an inverse relation. By increasing b,

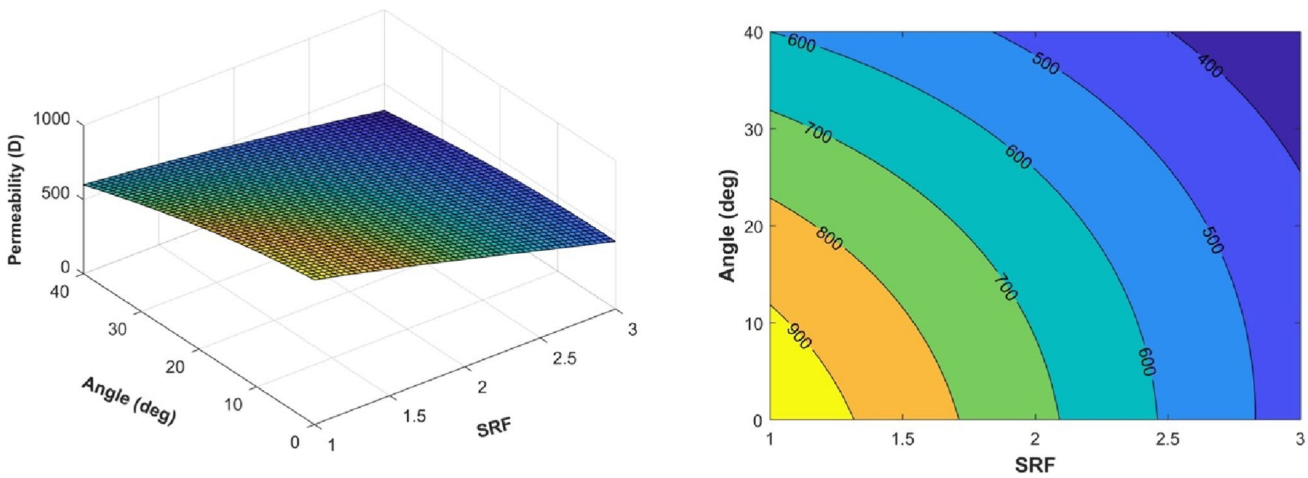

Fig. 6 3D plots and contour of fracture permeability versus SRF and angle at constant fracture opening (262.5 μm) and porosity (16.5%) values

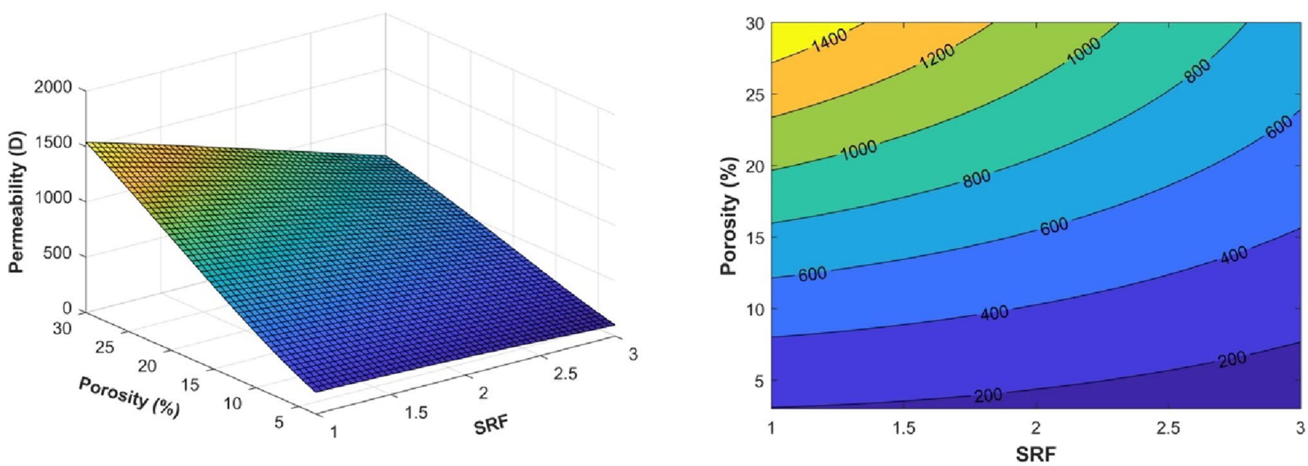

Fig. 7 3D plots and contour of fracture permeability versus SRF and porosity at constant fracture opening (262.5 μm) and angle (20°) values

the amount of the fluid that contributes to the flow would increase, and therefore, the same as φ, the pressure drop would decrease. Thus, by increasing b, the permeability would increase, which is in total agreement with the LCL relation. In addition, Fig. 9 shows the effect of b and φ. The result of this figure is similar to the previous ones.

In this study, the fluid flow through a 2D model and single rough fracture was investigated. However, other parameters like tortuosity may affect fracture permeability. Further studies are recommended to simulate fluid flow in 3D models and fracture networks.

Conclusions

In this study, an analysis was performed to study the fluid flow in rough fractures by computational fluid dynamics (CFD), and the effects of different parameters including SRF, φ, b, and θ were investigated. The following conclusions were drawn:

- The proposed response surface methodology (RSM) model could effectively predict the permeability of rough-walled fractures.
- The power-law model, optimized by the genetic algorithm, could accurately predict the fractures permeability.
- The results of the proposed correlations showed superiority over local cubic law (LCL) in the precise pre-

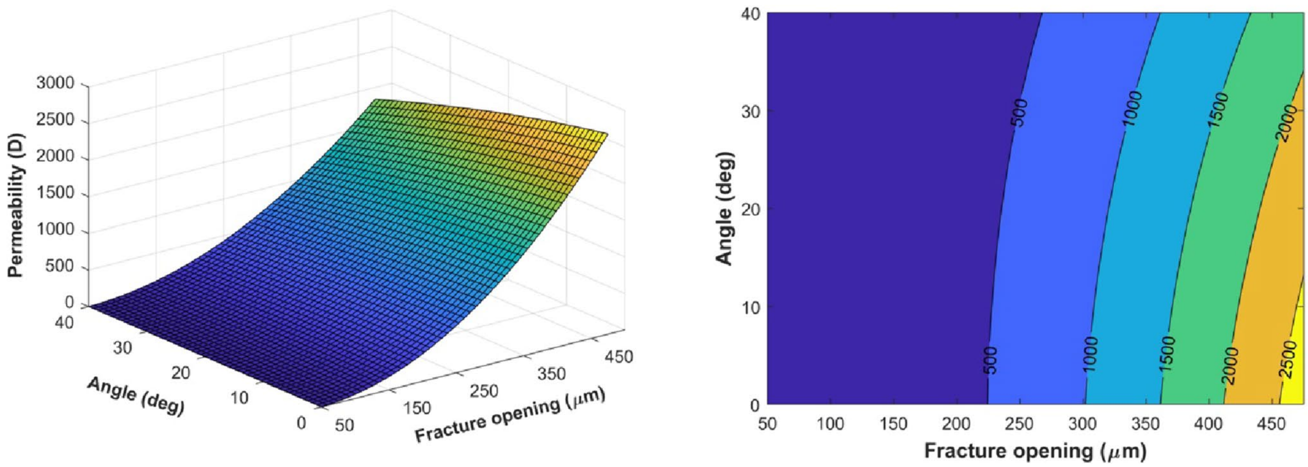

Fig. 8 3D plots and contour of fracture permeability versus fracture opening and the angle at constant SRF (2) and porosity (16.5%) values

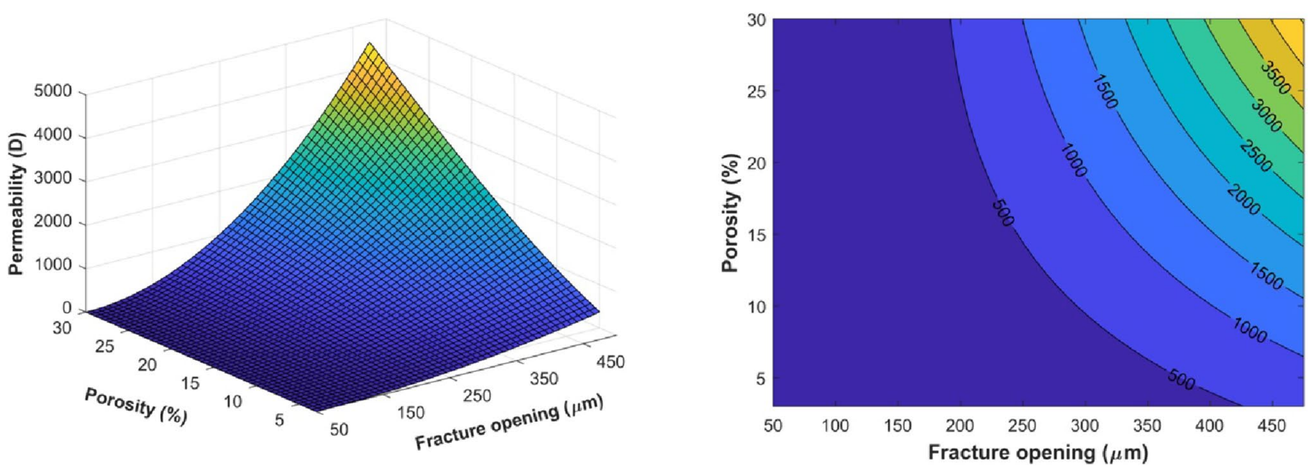

Fig. 9 3D plots and contour of fracture permeability versus fracture opening and porosity at constant SRF (2) and angle (20°) values

diction of fracture permeability in the presence of roughness. More precisely, the statistical analysis of the models indicated that the RSM model is the most accurate one (to find the fracture permeability). However, the power-law model has a simpler form than the RSM model.

- The proposed correlations are recommended to be used to estimate the permeability of hydraulic and natural fractures since surface roughness affects the fracture permeability, which the LCL model cannot capture its effect.
- In brief, the findings of this study contribute in several ways to our understanding of the considerable effect of roughness on the fluid flow in fractured reservoirs. Moreover, this work provides suitable correlations (RSM and power-law models) for the precise prediction of the permeability of the fracture in future works.

The main limitations of this work are as follows: fluid flow is considered laminar and other flow regimes are not modeled. Also, the utilized model was two-dimensional; three-dimensional models were not studied that results in ignoring the fracture tortuosity which influences fluid flow and our estimates of the fracture permeability. It is recommended to study three-dimensional models and investigate the effect of fracture tortuosity on permeability estimates in future works. Also, another future research direction can be studying the effect of roughness on fracture relative permeability under two-phase fluid flow. In addition, the results of simulation technique and local cubic law can be compared with experimental data.

Author contributions The manuscript was written through the contributions of all authors. All authors have approved the final version of the manuscript.

Funding No funding was received to assist with the preparation of this manuscript.

Declarations

Conflict of interest There is no conflict of interests to declare.

References

Abbasi J, Ghaedi M, Riazi M (2016) Discussion on similarity of recovery curves in scaling of imbibition process in fractured porous media. J Nat Gas Sci Eng 36:617–629. https://doi.org/10.1016/j.jngse.2016.11.017

Bagheri H, Falahat R (2022) Fracture permeability estimation utilizing conventional well logs and flow zone indicator. Pet Res 7:357–365. https://doi.org/10.1016/j.ptlrs.2021.11.004

Bararpour ST, Feylizadeh MR, Delparish A et al (2018) Investigation of 2-nitrophenol solar degradation in the simultaneous presence of K2S2O8 and H2O2: using experimental design and artificial neural network. J Clean Prod 176:1154–1162. https://doi.org/10.1016/j.jclepro.2017.11.191

Barton N, Choubey V (1977) Shear strength of rock joints in theory and practice. Int J Rock Mech Min Sci Geomech Abstr 10:1–54. https://doi.org/10.1016/0148-9062(78)90028-1

Bouquain J, Méheust Y, Bolster D, Davy P (2012) The impact of inertial effects on solute dispersion in a channel with periodically varying aperture. Phys Fluids 24:83602. https://doi.org/10.1063/1.4747458

Briggs S (2014) Impact of single fracture roughness on the flow

Crandall D, Bromhal G, Karpyn ZT (2010) Numerical simulations examining the relationship between wall-roughness and fluid flow in rock fractures. Int J Rock Mech Min Sci 47:784–796. https://doi.org/10.1016/j.ijrmms.2010.03.015

Deng H, Molins S, Trebotich D et al (2018) Pore-scale numerical investigation of the impacts of surface roughness: upscaling of reaction rates in rough fractures. Geochim Cosmochim Acta 239:374–389. https://doi.org/10.1016/j.gca.2018.08.005

Feilizadeh M, Alemzadeh I, Delparish A et al (2015a) Optimization of operating parameters for efficient photocatalytic inactivation of Escherichia coli based on a statistical design of experiments. Water Sci Technol 71:823–831. https://doi.org/10.2166/wst.2015.013

Feilizadeh M, Mul G, Vossoughi M (2015b) E. coli inactivation by visible light irradiation using a Fe–Cd/TiO2 photocatalyst: statistical analysis and optimization of operating parameters. Appl Catal B Environ 168–169:441–447. https://doi.org/10.1016/j.apcatb.2014.12.034

Feilizadeh M, Rahimi M, Zakeri SME et al (2017) Individual and interaction effects of operating parameters on the photocatalytic degradation under visible light illumination: response surface methodological approach. Can J Chem Eng 95:1228–1235. https://doi.org/10.1002/cjce.22808

Freites A, Geiger S, Corbett P (2019) Well test-derived permeability in naturally fractured reservoirs with heterogeneous and disconnected fractures. In: 81st EAGE Conference and Exhibition

Ghaedi M, Masihi M, Heinemann ZE, Ghazanfari MH (2015) History matching of naturally fractured reservoirs based on the recovery curve method. J Pet Sci Eng 126:211–221. https://doi.org/10.1016/j.petrol.2014.12.002

Glover PWJ, Matsuki K, Hikima R, Hayashi K (1998) Synthetic rough fractures in rocks. J Geophys Res Solid Earth 103:9609–9620. https://doi.org/10.1029/97JB02836

Guo P, Wang M, He M et al (2020) Experimental investigation on macroscopic behavior and microfluidic field of nonlinear flow in rough-walled artificial fracture models. Adv Water Resour 142:103637. https://doi.org/10.1016/j.advwatres.2020.103637

Gutfraind R, Hansen A (1995) Study of fracture permeability using lattice gas automata. Transp Porous Media 18:131–149. https://doi.org/10.1007/BF01064675

Hou P, Liang X, Zhang Y et al (2021) 3D multi-scale reconstruction of fractured shale and influence of fracture morphology on Shale gas flow. Nat Resour Res 30:2463–2481. https://doi.org/10.1007/s11053-021-09861-1

Javadi M, Sharifzadeh M, Shahriar K (2010) A new geometrical model for non-linear fluid flow through rough fractures. J Hydrol 389:18–30. https://doi.org/10.1016/j.jhydrol.2010.05.010

Ju Y, Zhang Q, Zheng J et al (2017) Fractal model and Lattice Boltzmann method for characterization of Non-Darcy flow in rough fractures. Sci Rep 7:41380. https://doi.org/10.1038/srep41380

Laongsakul P, Dürrast H (2011) Characterization of reservoir fractures using conventional geophysical logging. Songklanakarin J Sci Technol 33:237–246

Lei Q, Xu Y, Cai B et al (2022) Progress and prospects of horizontal well fracturing technology for shale oil and gas reservoirs. Pet Explor Dev 49:191–199. https://doi.org/10.1016/S1876-3804(22)60015-6

Lemonnier P, Bourbiaux B (2010) Simulation of naturally fractured reservoirs. state of the art: part 1 – physical mechanisms and simulator formulation. Oil Gas Sci Technol 65:239–262. https://doi.org/10.2516/ogst/2009066

Li L, Steefel CI, Yang L (2008) Scale dependence of mineral dissolution rates within single pores and fractures. Geochim Cosmochim Acta 72:360–377. https://doi.org/10.1016/j.gca.2007.10.027

Li T, Li Q, Hu Y et al (2021) Quantitative characterization of irregular microfracture network and its effect on the permeability of porous media. Pet Explor Dev 48:430–441. https://doi.org/10.1016/S1876-3804(21)60034-4

Liu R, Li B, Jiang Y (2016) Critical hydraulic gradient for nonlinear flow through rock fracture networks: the roles of aperture, surface roughness, and number of intersections. Adv Water Resour 88:53–65. https://doi.org/10.1016/j.advwatres.2015.12.002

Madadi M, Sahimi M (2003) Lattice Boltzmann simulation of fluid flow in fracture networks with rough, self-affine surfaces. Phys Rev E 67:26309. https://doi.org/10.1103/PhysRevE.67.026309

Mazaheri A, Memarian H, Tokhmechi B, Araabi BN (2015) Developing fracture measure as an index of fracture impact on well-logs. Energy Explor Exploit 33:555–574. https://doi.org/10.1260/0144-5987.33.4.555

Meakin P (1993) The growth of rough surfaces and interfaces. Phys Rep 235:189–289. https://doi.org/10.1016/0370-1573(93)90047-H

Mohammadi MM, Vossoughi M, Feilizadeh M et al (2014) Effects of electrophoretic deposition parameters on the photocatalytic activity of TiO2 films: optimization by response surface methodology. Colloids Surfaces A Physicochem Eng Asp 452:1–8. https://doi.org/10.1016/j.colsurfa.2014.03.048

Murata S, Saito T (2003) Estimation of Tortuosity of fluid flow through a single fracture. J Can Pet Technol. https://doi.org/10.2118/03-12-03

Patel SM, Sondergeld CH, Rai CS (2018) Hydraulic fracture permeability estimation using stimulation pressure data. Int J Rock Mech Min Sci 101:50–53. https://doi.org/10.1016/j.ijrmms.2017.11.013

Power WL, Tullis TE (1991) Euclidean and fractal models for the description of rock surface roughness. J Geophys Res Solid Earth 96:415–424. https://doi.org/10.1029/90JB02107

Renard F, Schmittbuhl J, Gratier JP et al (2004) Three-dimensional roughness of stylolites in limestones. J Geophys Res Solid Earth. https://doi.org/10.1029/2003JB002555

Renard F, Candela T, Bouchaud E (2013) Constant dimensionality of fault roughness from the scale of micro-fractures to the scale of continents. Geophys Res Lett 40:83–87. https://doi.org/10.1029/2012GL054143

Rezaei Niya SM, Selvadurai APS (2019) Correlation of joint roughness coefficient and permeability of a fracture. Int J Rock Mech Min Sci 113:150–162. https://doi.org/10.1016/j.ijrmms.2018.12.008

Sarkar S, Toksoz M, Burns D (2004) Fluid flow modeling in fractures. Earth Resources Laboratory. MIT Earth 1–41

Shalaby MR, Islam MA (2017) Fracture detection using conventional well logging in carbonate Matulla formation, Geisum oil field, southern Gulf of Suez. Egypt J Pet Explor Prod Technol 7:977–989. https://doi.org/10.1007/s13202-017-0343-1

Skjetne E, Hansen A, Gudmundsson J (1999) High-velocity flow in a rough fracture. J Fluid Mech 383:1–28. https://doi.org/10.1017/S0022112098002444

Snow DT (1969) Anisotropie permeability of fractured media. Water Resour Res 5:1273–1289. https://doi.org/10.1029/WR005i006p01273

Sund NL, Bolster D, Dawson C (2015) Upscaling transport of a reacting solute through a peridocially converging–diverging channel at pre-asymptotic times. J Contam Hydrol 182:1–15. https://doi.org/10.1016/j.jconhyd.2015.08.003

Talon L, Auradou H, Hansen A (2010) Permeability estimates of self-affine fracture faults based on generalization of the bottleneck concept. Water Resour Res. https://doi.org/10.1029/2009WR008404

Tarek A (2010) Reservoir Engineering Handbook, 4th edn. Gulf Professional Publishing

Toghraie D, Hekmatifar M, Salehipour Y, Afrand M (2019) Molecular dynamics simulation of Couette and Poiseuille water-copper nanofluid flows in rough and smooth nanochannels with different roughness configurations. Chem Phys 527:110505. https://doi.org/10.1016/j.chemphys.2019.110505

Tsang YW, Witherspoon PA (1981) Hydromechanical behavior of a deformable rock fracture subject to normal stress. J Geophys Res Solid Earth 86:9287–9298. https://doi.org/10.1029/JB086iB10p09287

Tsang YW, Tsang CF, Neretnieks I, Moreno L (1988) Flow and tracer transport in fractured media: a variable aperture channel model and its properties. Water Resour Res 24:2049–2060. https://doi.org/10.1029/WR024i012p02049

Van Golf-Racht T (1982) Fundamentals of fractured reservoir engineering. Elsevier Scientic Publishing Company

Versteeg HK (1995) An introduction to computational fluid dynamics; the finite volume method. Pearson

Wang L, Cardenas MB, Slottke DT et al (2015) Modification of the local cubic law of fracture flow for weak inertia, tortuosity, and roughness. Water Resour Res 51:2064–2080. https://doi.org/10.1002/2014WR015815

Wang M, Chen YF, Ma GW et al (2016) Influence of surface roughness on nonlinear flow behaviors in 3D self-affine rough fractures: Lattice Boltzmann simulations. Adv Water Resour 96:373–388. https://doi.org/10.1016/j.advwatres.2016.08.006

Wang Z, Xu C, Dowd P (2018) A modified cubic law for single-phase saturated laminar flow in rough rock fractures. Int J Rock Mech Min Sci 103:107–115. https://doi.org/10.1016/j.ijrmms.2017.12.002

Wang K, Zhang G, Wang Y et al (2022) A numerical investigation of hydraulic fracturing on coal seam permeability based on PFC-COMSOL coupling method. Int J Coal Sci Technol 9:10. https://doi.org/10.1007/s40789-022-00484-2

Xu H, Jiao Z, Zhang Z et al (2021) Prediction of methane hydrate formation conditions in salt water using machine learning algorithms. Comput Chem Eng 151:107358. https://doi.org/10.1016/j.compchemeng.2021.107358

Yousefzadeh R, Ahmadi M (2023) Improved history matching of channelized reservoirs using a novel deep learning-based parametrization method. Geoenergy Sci Eng 229:212113. https://doi.org/10.1016/j.geoen.2023.212113

Yousefzadeh R, Kazemi A, Ahmadi M, Gholinezhad J (2023) History matching and Robust optimization using proxies. Springer, Cham, pp 115–132

Zhang L, Hascakir B (2021) A review of issues, characteristics, and management for wastewater due to hydraulic fracturing in the US. J Pet Sci Eng 202:108536. https://doi.org/10.1016/j.petrol.2021.108536

Zhang X, Knackstedt MA, Sahimi M (1996) Fluid flow across mass fractals and self-affine surfaces. Phys A Stat Mech Appl 233:835–847. https://doi.org/10.1016/S0378-4371(96)00203-8

Zimmerman RW, Kumar S, Bodvarsson GS (1991) Lubrication theory analysis of the permeability of rough-walled fractures. Int J Rock Mech Min Sci Geomech Abstr 28:325–331. https://doi.org/10.1016/0148-9062(92)91194-A